Strathprints Institutional Repository

Lattice ellipsoidal statistical BGK model for thermal non-equilibrium flows

Jianping Meng[1], Yonghao Zhang[1], Nicolas G. Hadjiconstantinou[2], Gregg A. Radtke[2] and Xiaowen Shan[3]

[1]Department of Mechanical & Aerospace Engineering, University of Strathclyde, Glasgow G1 1XJ, UK

[2]Department of Mechanical Engineering, Massachusetts Institute of Technology, Cambridge, Massachusetts 02139, USA

[3]Exa Corporation, 55 Network Drive, Burlington, Massachusetts 01803, USA

(Received 11 September 2012)

A thermal lattice Boltzmann model is constructed on the basis of the ellipsoidal statistical Bhatnagar-Gross-Krook (ES-BGK) collision operator via the Hermite moment representation. The resulting lattice ES-BGK model uses a single distribution function and features an adjustable Prandtl number. Numerical simulations show that using a moderate discrete velocity set, this model can accurately recover steady and transient solutions of the ES-BGK equation in the slip-flow and early transition regimes in the small Mach number limit that is typical of microscale problems of practical interest. In the transition regime in particular, comparisons with numerical solutions of the ES-BGK model, direct Monte Carlo and low-variance deviational Monte Carlo simulations show good accuracy for values of the Knudsen number up to approximately 0.5. On the other hand, highly non-equilibrium phenomena characterized by high Mach numbers, such as viscous heating and force-driven Poiseuille flow for large values of the driving force, are more difficult to capture quantitatively in the transition regime using discretizations that have been chosen with computational efficiency in mind such as the one used here, although improved accuracy is observed as the number of discrete velocities is increased.

1. Introduction

The lattice Boltzmann (LB) method has been successful in simulating isothermal (athermal) flows; however, thermal flows still remain a challenge, despite significant efforts from a number of research groups (see Shim & Gatignol 2011; Sbragaglia *et al.* 2009; Scagliarini *et al.* 2010; Prasianakis *et al.* 2009; Prasianakis & Karlin 2008; Watari 2009; Gonnella *et al.* 2007; Zheng *et al.* 2010; Guo *et al.* 2007; Shan & Chen 2007; Watari & Tsutahara 2003; Prasianakis & Karlin 2007; Lallemand & Luo 2003; Chen & Doolen 1998). Recent approaches fall into two broad categories: the high-order approach (e.g., Sbragaglia *et al.* 2009; Shan & Chen 2007; Watari & Tsutahara 2003) and the double-distribution-function approach (e.g., He *et al.* 1998; Shan 1997). As a direct extension of the isothermal LB model, the high-order model only uses one distribution function while retaining high-order terms in the equilibrium distribution function to recover the full Navier-Stokes (NS) equations. Unfortunately, this approach requires a richer velocity space and as a result suffers in terms of simplicity and in some cases numerical instability†. By contrast, in the double-distribution-function approach, two distribution functions

† We also note some efforts on constructing single-distribution-function thermal models using standard lattices e.g. a 2 dimensional model with nine discrete velocities (see Prasianakis & Karlin 2007).

are utilized: one for the velocity field and the other for the temperature field. As a result, high-order terms can be avoided and the standard lattice can be used. In addition, this approach is numerically more stable. However, to utilize the standard lattice, the energy and momentum transport equation need to be decoupled through the Boussinesq approximation (cf. Guo *et al.* 2007); in this case the double distribution approach does not recover the full NS equations in a strict sense.

In addition to heat transfer, kinetic effects can make flows even more complex. For example, for gaseous flows at the microscale, kinetic effects have to be taken into account as the Knudsen number (Kn, the ratio of the mean free path and the characteristic length) becomes finite (Hadjiconstantinou 2006). Due to its kinetic origins, the LB method has been shown to be able to describe moderately complex kinetic effects (see, e.g., Zhang *et al.* 2005; Toschi & Succi 2005; Sbragaglia & Succi 2005, 2006; Tang *et al.* 2008*b*; Zhang *et al.* 2006; Shan *et al.* 2006; Ansumali *et al.* 2007; Kim *et al.* 2008*a*; Yudistiawan *et al.* 2008; Guo *et al.* 2006; Succi 2002; Kim *et al.* 2008*b*; Tang *et al.* 2008*a*; Tian *et al.* 2007). Particularly, as the LB method can be considered as an approximation to the Boltzmann-BGK equation, high-order models should, in principle, be able to go beyond NS hydrodynamics (Shan *et al.* 2006; Meng & Zhang 2011*a*). Both analytical and numerical analysis have shown that using a generous discrete velocity set, LB models can capture kinetic effects including the Knudsen layer qualitatively and provide reasonably accurate results for a range of isothermal problems (Kim *et al.* 2008*a*; Yudistiawan *et al.* 2008); also, as expected, more discrete velocities generally give better predictions (Meng & Zhang 2011*a*). When gas-surface interactions are concerned, discrete velocity sets from even-order Hermite polynomials typically perform better (Meng & Zhang 2011*b*). For thermal rarefied flows, despite that the velocity-slip and temperature-jump problems have been investigated using a high-order LB model (Watari 2009), significant effort is still required to develop robust LB methods for modeling general thermal non-equilibrium flows of engineering interest.

The Hermite expansion provides a systematic approach to derivation of the LB models for representing the NS hydrodynamic systems and beyond (Shan *et al.* 2006). The usage of the Hermite expansion was pioneered by Grad (1958, 1949) for approximating the Boltzmann equation. An important feature of Hermite polynomials is that the expansion coefficients correspond directly to moments of the distribution function. In addition, the truncation of higher-order terms do not directly alter the lower-order velocity moments of the distribution function. In his famous paper, Grad kept the first thirteen Hermite coefficients and obtained the well known 13-moment system (Grad 1949). This system contains physics beyond the NS equation. However, a significant weakness of Grad's 13-moment system is its inability to describe smooth shock structures above a critical Mach number. Also, this system is not easily related a priori to the Knudsen number. As a result, significant effort has been devoted towards the development of an improved moment system in the last decade. Regularization for Grad's 13 moment system (i.e., the so-called R13 system) has been introduced on the basis of a Chapman-Enskog expansion around a non-equilibrium state (Struchtrup & Torrilhon 2003; Struchtrup 2005, 2004). The related issues associated with the numerical scheme and boundary conditions have then been discussed by Torrilhon & Struchtrup (2008) and Gu & Emerson (2007). A series of analytical solutions were also obtained and compared to the kinetic solutions (see Taheri *et al.* 2009; Taheri & Struchtrup 2010). In addition to the R13 system, higher-order moment equation models have also been developed (Gu & Emerson 2009).

Inspired by Grad's work, the Hermite expansion has been used to derive new LB models (Shan *et al.* 2006; Shan & He 1998). It was shown that the truncation of the Hermite expansion is equivalent to evaluating the distribution function at the chosen order of the

discrete velocities. Thus, the resulting LB models can describe gaseous systems at the corresponding level. However, contrary to Grad's approach, the governing equation of LB models is presented in a much simpler form (e.g., the linear convective term) as the evolution is accomplished at the distribution function level rather than the state-variable level. Therefore, the LB model has some advantages, e.g., straightforward numerical implementation and code parallelisation.

In this work, we establish a thermal LB model based on the ellipsoidal statistical Bhatnagar-Gross-Krook (ES-BGK) equation following the systematic high-order procedure of the Hermite expansion. The resulting model features an adjustable Prandtl number in contrast to the BGK model whose Prandtl number is fixed at 1. We validate our model using shear-driven (Couette) flows, Fourier flows and unsteady boundary heating problems in the small Mach-number limit over a range of Knudsen numbers. Using only a moderate set of discrete velocities, we find very good agreement with benchmark solutions. We also show that, with the same moderate discrete velocity set, highly non-equilibrium problems characterized by high Mach numbers, such as force-driven Poiseuille flow for large values of the driving force, are captured accurately in the slip-flow regime and with good qualitative accuracy in the transition regime. Better accuracy requires a higher number of discrete velocities, in addition to higher-order Hermite expansion.

2. Thermal lattice Boltzmann model

2.1. *The ES-BGK equation*

The difficulty associated with solving the Boltzmann equation is mainly due to the collision term. To reduce the complexity, the collision term may be replaced by a simple statistical model that preserves the conservation laws of mass, momentum and energy. The most commonly-used model is known as the Bhatnagar-Gross-Krook (BGK) collision operator, which is often used in constructing lattice Boltzmann models. Despite its success, the BGK model suffers from a number of drawbacks: specifically, it yields a fixed Prandtl number (Pr) of unity, while the correct value for a monatomic gas is close to 2/3. To address this limitation, Holway (1966) proposed ES-BGK model that replaces the Maxwellian distribution of the standard BGK equation with an anisotropic Gaussian distribution, which can be written as

$$\frac{\partial \hat{f}}{\partial \hat{t}} + \hat{c}_i \frac{\partial \hat{f}}{\partial \hat{x}_i} + \hat{g}_i \frac{\partial \hat{f}}{\partial \hat{c}_i} = -\frac{1}{\hat{\tau}}(\hat{f} - \hat{f}_{ES}), \tag{2.1}$$

where $\hat{f}$ denotes the single-particle distribution function, $\hat{c}_i$ the phase (particle) velocity, $\hat{g}_i$ the body force and $\hat{\tau}$ the mean relaxation time which is assumed to be independent of particle velocity. The anisotropic Gaussian distribution can be written as

$$\hat{f}_{ES} = \hat{\rho} \frac{1}{\sqrt{\det[2\pi \hat{\lambda}_{ij}]}} \exp\left[-\frac{1}{2}\hat{\lambda}_{ij}^{-1} \hat{C}_i \hat{C}_j\right], \tag{2.2}$$

where $\hat{\lambda}_{ij} = R\hat{T}\delta_{ij} + (b\hat{\sigma}_{ij})/\hat{\rho}$ and R is the gas constant. Macroscopic quantities, such as density $\hat{\rho}$, velocity $\hat{\boldsymbol{u}}$, shear stress $\hat{\boldsymbol{\sigma}}$, temperature $\hat{T}$ and heat flux $\hat{\boldsymbol{q}}$, can be obtained by

integrating the distribution function over the velocity space, i.e.

$$\begin{bmatrix} \hat{\rho} \\ \hat{\rho}\hat{u}_i \\ \hat{\sigma}_{ij} \\ \hat{q}_i \\ \hat{\rho}D R\hat{T} \end{bmatrix} = \int \hat{f} \begin{bmatrix} 1 \\ \hat{c}_i \\ \hat{C}_{<i}\hat{C}_{j>} \\ \frac{1}{2}\hat{C}_i\hat{C}_j\hat{C}_j \\ \hat{C}_i\hat{C}_i \end{bmatrix} d\hat{\boldsymbol{c}}, \tag{2.3}$$

where $\hat{C}_i = \hat{c}_i - \hat{u}_i$ is the particle peculiar velocity and the angle bracket denotes the trace-free tensors (see Struchtrup 2005*b*, Appendix A.2.2). The pressure $\hat{p}$ can be related to the density and temperature by the equation of state

$$\hat{p} = \hat{\rho} R \hat{T}. \tag{2.4}$$

As $\hat{\lambda}_{ij}^{-1}$ (the inverse of the matrix) must be positive definite, b is restricted to $-\frac{1}{2} \leqslant b \leqslant 1$. The exact values of b and $\hat{\tau}$ can be determined by the Boltzmann integral with a known inter-molecular force law or experimental data. In this work, experimental values will be used. The Navier Stokes equations can be derived (Holway 1966) using a Chapman-Enskog expansion. The viscosity and thermal conduction coefficients can be written as $\hat{\mu} = (\hat{p}\hat{\tau})/(1-b)$ and $\hat{\kappa} = \hat{p}R(D+2)\hat{\tau}/2$, respectively, where D is the spatial dimension. Therefore, the Prandtl number is given by $Pr = 1/(1-b)$ and can be adjusted via the free parameter b. For thermal flows, viscosity depends on temperature, and can be expressed as $\hat{\mu}/\mu_0 = (\hat{T}/T_0)^{\varpi}$, where ϖ is related to the molecular interaction model, varying from 0.5 for hard-sphere molecular interactions to 1 for Maxwellian interactions. Therefore, in general, $\hat{\tau}$ may be taken to be a function of temperature.

The ES-BGK model has received renewed attention, in part because the associated H theorem was recently proven (Andries *et al.* 2000). Several studies have shown that it can provide reasonable accuracy for modeling transport in simple rarefied flows (Andries *et al.* 2002; Han *et al.* 2007; Graur & Polikarpov 2009; Han *et al.* 2011; Mieussens & Struchtrup 2004; Gallis & Torczynski 2011; Garzó & Andrés Santos 1995). In the following, we will develop a thermal LB model based on the ES-BGK equation using the Hermite moment representation (Shan *et al.* 2006); we will refer to the resulting LB method as the lattice ES-BGK model. In order to separate the numerical error arising from the LB method from the modeling error associated with approximating the hard-sphere operator with the ES-BGK model, we will also present *numerical* solutions of the Boltzmann equation with the ES-BGK collision operator obtained using the finite difference/discrete velocity method presented in Aoki *et al.* (2002). Although this method is not practical for problems of engineering interest due to the high dimensionality associated with the very fine discretization of the velocity space, it can be used to obtain accurate solutions of the ES-BGK equation in the one-dimensional benchmark problems considered here. In order to differentiate from our lattice-based solutions, we will refer to the ones obtained by the finite difference/discrete velocity method as *numerical*.

2.2. *Derivation of the lattice ES-BGK equation*

Shan *et al.* (2006) have shown that a hierarchy of different order LB models can be systematically derived from the BGK equation via the Hermite expansion, which can be regarded as approximations to the BGK equation. Fluid flows can then be described at the kinetic level with various discrete velocity sets. This procedure can also be used to derive the lattice ES-BGK model. For convenience, we use the following non-dimensional

system,

$$x_i = \frac{\hat{x}_i}{L}, u_i = \frac{\hat{u}_i}{\sqrt{RT_0}}, t = \frac{\sqrt{RT_0}\hat{t}}{L}, g_i = \frac{L\hat{g}_i}{RT_0}, c_i = \frac{\hat{c}_i}{\sqrt{RT_0}}, T = \frac{\hat{T}}{T_0},$$

$$\tau = \frac{\sqrt{RT_0}\hat{\tau}}{L}, f = \frac{\hat{f}(RT_0)^{D/2}}{\rho_0}, \rho = \frac{\hat{\rho}}{\rho_0}, p = \frac{\hat{p}}{p_0}, \mu = \frac{\hat{\mu}}{\mu_0}, q_i = \frac{\hat{q}_i}{p_0\sqrt{RT_0}}, \sigma_{ij} = \frac{\hat{\sigma}_{ij}}{p_0}.$$

The temperature and state equations become

$$DT = \frac{1}{\rho}\int f C_i C_i d\boldsymbol{c},$$

$$p = \rho T,$$

while the other equations are still in the same form. The non-dimensional relaxation time can be written explicitly as

$$\tau = \frac{\mu_0\sqrt{RT_0}}{p_0 L}\frac{\mu}{Prp} = \frac{Kn}{Pr}\frac{\mu}{p},$$

and the Knudsen number is defined as

$$Kn = \frac{\mu_0\sqrt{RT_0}}{p_0 L}.$$

To solve Eq.(2.1), the distribution function is first projected onto a functional space spanned by the Hermite basis. If a Gauss-Hermite quadrature of a degree $\geqslant 2N$ is chosen, then the first N velocity moments of the distribution function are retained (see Shan *et al.* 2006, P.420). Therefore, the distribution function is essentially approximated as

$$f(\boldsymbol{x}, \boldsymbol{c}, t) \approx \omega(\boldsymbol{c}) \sum_{n=0}^{N} \frac{1}{n!} \boldsymbol{a}^{(n)}(\boldsymbol{x}, t) : \boldsymbol{\chi}^{(n)}(\boldsymbol{c}), \tag{2.5}$$

and the coefficients $\boldsymbol{a}^{(n)}$ are calculated from

$$\boldsymbol{a}^{(n)} = \int f \boldsymbol{\chi}^{(n)} d\boldsymbol{c} \tag{2.6}$$

where $\boldsymbol{\chi}^{(n)}$ is the n-th order Hermite polynomial and $\omega(\mathbf{c})$ is the weight function.

The key step is to expand the anisotropic Gaussian distribution as

$$f_{ES} \approx f_{ES}^{N} = \omega(\boldsymbol{c}) \sum_{n=0}^{N} \frac{1}{n!} \boldsymbol{a}_{ES}^{(n)} : \boldsymbol{\chi}^{(n)}(\boldsymbol{c}), \tag{2.7}$$

where

$$\boldsymbol{a}_{ES}^{(n)} = \int f_{ES} \boldsymbol{\chi}^{(n)} d\boldsymbol{c} \approx \sum_{\alpha=1}^{d} \frac{w_\alpha}{\omega(\boldsymbol{c}_\alpha)} f_{ES}^{N} \boldsymbol{\chi}^{n}(\boldsymbol{c}_\alpha), \tag{2.8}$$

and w_α and $\boldsymbol{c}_\alpha$, $\alpha = 1, \cdots, d$, are the weights and abscissae of a Gauss-Hermite quadrature. For the anisotropic distribution, the first a few coefficients are given by

$$a_{ES}^{(0)} = \rho, \tag{2.9}$$

$$a_{ES,i}^{(1)} = \rho u_i, \tag{2.10}$$

$$a_{ES,ij}^{(2)} = \rho(u_i u_j + \lambda_{ij} - \delta_{ij}), \tag{2.11}$$

$$a^{(3)}_{ES,ijk} = \rho(u_i u_j u_k + \lambda_{ij} u_k + \lambda_{ik} u_j + \lambda_{jk} u_i - \delta_{ij} u_k - \delta_{ik} u_j - \delta_{jk} u_i), \tag{2.12}$$

$$\begin{aligned} a^{(4)}_{ES,ijkl} = \rho[&u_i u_j u_l u_k + (\lambda_{il} - \delta_{il}) u_j u_k + (\lambda_{ij} - \delta_{ij}) u_l u_k + (\lambda_{ik} - \delta_{ik}) u_j u_l \\ &+ (\lambda_{jl} - \delta_{jl}) u_i u_k + (\lambda_{jk} - \delta_{jk}) u_i u_l + (\lambda_{kl} - \delta_{kl}) u_i u_j \\ &+ (\lambda_{ij} - \delta_{ij})(\lambda_{kl} - \delta_{kl}) + (\lambda_{ik} - \delta_{ik})(\lambda_{jl} - \delta_{jl}) + (\lambda_{il} - \delta_{il})(\lambda_{kj} - \delta_{kj})]. \end{aligned} \tag{2.13}$$

The body force term $F(\boldsymbol{x}, \boldsymbol{c}, t) = -\boldsymbol{g} \cdot \nabla_c f$ can be approximated as:

$$F(\boldsymbol{x}, \boldsymbol{c}, t) = \omega \sum_{n=1}^{N} \frac{1}{(n-1)!} \boldsymbol{g} \boldsymbol{a}^{(n-1)} : \boldsymbol{\chi}^{(n)}. \tag{2.14}$$

Although Eq. (2.2) has an infinite Hermite expansion, a LB model is built under the assumption that to some level of approximation only the leading terms contribute explicitly to the hydrodynamics (see Shan *et al.* 2006) and thus the infinite series can be truncated. In this work, a 4th-order Hermite expansion will be used.

Given the above discussion, the ES-BGK equation Eq.(2.1) can be rewritten in its truncated form, i.e.,

$$\frac{\partial f}{\partial t} + c_i \frac{\partial f}{\partial x_i} = -\frac{1}{\tau}(f - f^N_{ES}) + F. \tag{2.15}$$

For a 4th-order expansion, a discrete velocity set with 9th-order or higher accuracy is required (Shan *et al.* 2006). There are a number of ways of constructing a high-order discrete velocity set (Shan *et al.* 2006; Shan 2010; Chikatamarla & Karlin 2009, 2006). A straightforward approach is to utilize the roots of the Hermite polynomial. In one-dimension, the discrete velocities c_α are just the roots of the Hermite polynomials, and the corresponding weights are determined by:

$$w_\alpha = \frac{n!}{[n\chi^{n-1}(c_\alpha)]^2}. \tag{2.16}$$

Another useful procedure is to utilize the entropy construction (cf. Chikatamarla & Karlin 2006, 2009). Given one-dimensional velocity sets, those of the higher-dimension can be constructed using the "production" formulae (Shan *et al.* 2006). Once the discrete velocity set is chosen, the governing equation of the lattice ES-BGK model can be written as

$$\frac{\partial f_\alpha}{\partial t} + c_{\alpha,i} \frac{\partial f_\alpha}{\partial x_i} = -\frac{1}{\tau}(f_\alpha - f_{ES,\alpha}) + g_\alpha, \tag{2.17}$$

where $f_\alpha = \frac{w_\alpha f(\boldsymbol{x}, \boldsymbol{c}_\alpha, t)}{\omega(\boldsymbol{c}_\alpha)}$, $f_{ES,\alpha} = \frac{w_\alpha f_{ES}(\boldsymbol{x}, \boldsymbol{c}_\alpha, t)}{\omega(\boldsymbol{c}_\alpha)}$ and $g_\alpha = \frac{w_\alpha F(\boldsymbol{x}, \boldsymbol{c}_\alpha, t)}{\omega(\boldsymbol{c}_\alpha)}$.

2.3. *Remarks on the accuracy beyond Navier-Stokes*

As the distribution functions f and f_{ES} are approximated and evaluated at the Gauss-Hermite quadrature points, cf Eq.(2.5), we can relate the chosen Gauss-Hermite quadrature to the approximated moments of the distribution function. Generally speaking, more discrete velocities mean higher-order moments can be obtained more accurately. With sufficiently accurate quadrature and retaining increasingly high-order terms of the expanded f_{ES}, the LB model is approaching to the original ES-BGK equation (cf Fig.20).

When the Chapman-Enskog expansion is valid, we can evaluate model accuracy in terms of the Knudsen number. According the Chapman-Enskog expansion, the distribution function f is assumed to be a asymptotic series expanded in powers of the (formal) small parameter ϵ (see Struchtrup 2005*b*, Chapter 4),

$$f = f^0 + \epsilon f^{(1)} + \epsilon^2 f^{(2)} + \cdots \tag{2.18}$$

where ϵ plays the role of the Knudsen number; f^0 is the truncation of the Maxwellian f_M, its first four Hermite coefficients were already given by Shan *et al.* (2006), cf. Eq.(3.12). Furthermore the time and spatial variations are also measured in powers of ϵ, i.e.,

$$\partial_t = \epsilon\partial_t^{(0)} + \epsilon^2\partial_t^{(1)} + \cdots \tag{2.19}$$

and $\boldsymbol{\nabla} = \epsilon\boldsymbol{\nabla}$ (Shan *et al.* 2006). Considering the form of f^0, f_{ES}^N can be written as

$$f_{ES}^N = f^0 + \omega\left[\frac{1}{2}b\sigma_{ij}\chi_{ij}^{(2)} + \frac{1}{6}(\sigma_{ij}u_k + \sigma_{ik}u_j + \sigma_{jk}u_i)\chi_{ijk}^{(3)} + \cdots\right]. \tag{2.20}$$

The shear stress σ_{ij} should be also expanded as

$$\sigma_{ij} = \epsilon\sigma_{ij}^{(1)} + \epsilon^2\sigma_{ij}^{(2)} + \cdots, \tag{2.21}$$

and f_{ES}^N can thereby be written as,

$$f_{ES}^N = f^0 + \epsilon f_{ES}^{N,(1)} + \epsilon^2 f_{ES}^{N,(2)} + \cdots, \tag{2.22}$$

where

$$f_{ES}^{N,(1)} = \omega\left[\frac{1}{2}b\sigma_{ij}^{(1)}\chi_{ij}^{(2)} + \frac{1}{6}(\sigma_{ij}^{(1)}u_k + \sigma_{ik}^{(1)}u_j + \sigma_{jk}^{(1)}u_i)\chi_{ijk}^{(3)} + \cdots\right], \tag{2.23}$$

and

$$f_{ES}^{N,(2)} = \omega\left[\frac{1}{2}b\sigma_{ij}^{(2)}\chi_{ij}^{(2)} + \frac{1}{6}(\sigma_{ij}^{(2)}u_k + \sigma_{ik}^{(2)}u_j + \sigma_{jk}^{(2)}u_i)\chi_{ijk}^{(3)} + \cdots\right]. \tag{2.24}$$

By matching the terms in the same powers of ϵ, we can have the solution for the two leading orders, namely the NS order

$$f^{(1)} = f_{ES}^{N,(1)} - \tau(\partial_t^{(0)} + \boldsymbol{c}\cdot\boldsymbol{\nabla} + \boldsymbol{g}\cdot\boldsymbol{\nabla}_c)f^{(0)} \tag{2.25}$$

and the Burnett order

$$f^{(2)} = f_{ES}^{N,(2)} - \tau[(\partial_t^{(0)} + \boldsymbol{c}\cdot\boldsymbol{\nabla} + \boldsymbol{g}\cdot\boldsymbol{\nabla}_c)f^{(1)} + \partial_t^1 f^0]. \tag{2.26}$$

According to the above two equations, it is tedious to calculate the explicit form of $f^{(1)}$ and $f^{(2)}$. However, for the current purpose, we only need to know their highest order as a Hermite polynomial of the particle velocity $\boldsymbol{c}$. To determine the highest-order, we notice that the operators ∂_t^0 and ∂_t^1 do not alter the order while $\boldsymbol{c}\cdot\boldsymbol{\nabla}$ or $\boldsymbol{\nabla}_c$ operation increase the order by one. Therefore, the Burnett order solution $f^{(2)}$ is a polynomial of $\boldsymbol{c}$ of two-order higher than f_{ES}^N. If it is desired, the relation for the higher-order solution can be obtained similarly. Here we restrict the discussion on the first two orders.

With the above discussion, we can estimate the accuracy level with the chosen expansion order and quadrature. As the fourth-order terms of $\boldsymbol{c}$ in f_{ES} are retained, the Burnett-order solution of the distribution function can be represented by a sixth-order polynomial. For the heat flux, a third-order velocity moment, to be calculated with the Burnett level of accuracy, the chosen quadrature has to be accurate for an integration over the full space for a ninth-order polynomial. Hence, according the Gaussian quadrature rule (cf., Shan *et al.* 2006, Appendix in), it is necessary to adopt a quadrature with an algebraic degree of precision beyond the ninth-order. However, as the ninth-order quadrature has some defect in describing the gas-wall interactions (Meng & Zhang 2011*b*), an 11th-order quadrature is chosen in this work. On the other hand, the 11th-order is also expected to deal well with the integration for the transport flux of heat flux (a forth order moment) at the Burnett lever, which may help to improve the accuracy for the heat flux.

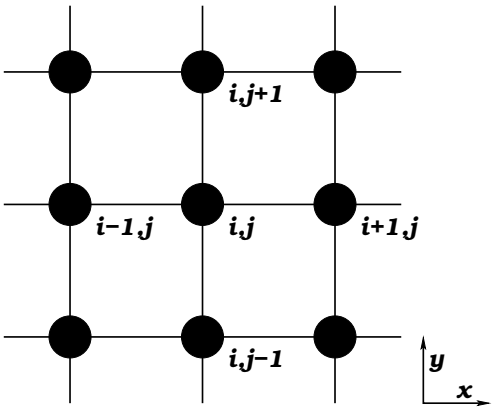

FIGURE 1. Schematic diagram of square lattices.

It is worth noting again that the above analysis relies on the validity of the Chanpman-Enskog expansion. Consequently, one should be careful when interpreting the above conclusion for large Knudsen numbers. Furthermore, it may be better to understand the requirement on the quadrature for the corresponding accuracy as necessary rather than sufficient. Nevertheless, the above discussion is informative to understand the capability of the LB model, which can be seen in numerical simulations below.

3. Numerical implementation

3.1. *Scheme*

To solve Eq. (2.17), various numerical schemes can be used, depending on the characteristics of the problem of interest. Typically, if a first-order upwind finite difference is chosen, we have a standard stream-collision scheme.

As flows with various Knudsen numbers will be considered in the following simulations, the numerical scheme has to be carefully chosen to cope with discontinuities at the system boundaries caused by rarefaction (Hadjiconstantinou 2006). In particular, in order to intrinsically describe the gas-surface interaction, the kinetic boundary condition should be accurately implemented in the numerical scheme. Meanwhile, there is still no general and accurate implementation of the standard stream-collision scheme for high-order models, especially for rarefied flows. On the other hand, for high-order LB models, the discrete velocity points may not coincide with the lattice points, which makes the standard stream-collision procedure impossible. Therefore, in the interest of simplicity, a finite difference formulation has been chosen and more specifically, a 1st-order forward Euler method is coupled to a 2nd-order total variation diminishing (TVD) scheme (Kim *et al.* 2008*a*; Sofonea 2009; Toro 2009).

The resulting scheme can be summarized as follows. Let $f_{\alpha,i}^{n,j}$ denote the distribution function value f_α at the node (x_i, y_j) at the n-th time step (see Fig.1). The distribution function update can be written as

$$\begin{aligned} f_{\alpha,i}^{n+1,j} = f_{\alpha,i}^{n,j} &- \frac{c_{\alpha x}\delta_t}{\delta_x}\left[\mathcal{F}_{\alpha,i+1/2}^{n,j} - \mathcal{F}_{\alpha,i-1/2}^{n,j}\right] \\ &- \frac{c_{\alpha y}\delta_t}{\delta_y}\left[\mathcal{F}_{\alpha,i}^{n,j+1/2} - \mathcal{F}_{\alpha,i}^{n,j-1/2}\right] \\ &+ \frac{\delta_t}{\tau}(f_{\alpha,i}^{ES,n,j} - f_{\alpha,i}^{n,j}) + g_\alpha\delta_t, \end{aligned} \tag{3.1}$$

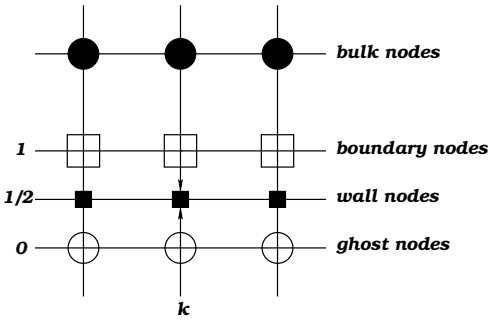

FIGURE 2. Schematic illustration of wall boundary treatment.

where δ_x and δ_y are the grid spacing in the x and y directions, respectively, and δ_t is the time step; $c_{\alpha x}$ and $c_{\alpha y}$ denote the particle velocity components at the x and y coordinates. The outgoing and incoming fluxes at the node (i, j) (see Fig.1) are

$$\mathcal{F}^{n,j}_{\alpha,i+1/2} = f^{n,j}_{\alpha,i} + \frac{1}{2}\left(1 - \frac{c_{\alpha x}\delta_t}{\delta_x}\right)\left[f^{n,j}_{\alpha,i+1} - f^{n,j}_{\alpha,i}\right]\Psi\left(\Theta^{n}_{\alpha,i}\right), \tag{3.2}$$

$$\mathcal{F}^{n,j}_{\alpha,i-1/2} = \mathcal{F}^{n,j}_{\alpha,(i-1)+1/2}, \tag{3.3}$$

$$\mathcal{F}^{n,j+1/2}_{\alpha,i} = f^{n,j}_{\alpha,i} + \frac{1}{2}\left(1 - \frac{c_{\alpha y}\delta_t}{\delta_y}\right)\left[f^{n,j+1}_{\alpha,i} - f^{n,j}_{\alpha,i}\right]\Psi\left(\Theta^{n,j}_{\alpha}\right), \tag{3.4}$$

$$\mathcal{F}^{n,j-1/2}_{\alpha,i} = \mathcal{F}^{n,(j-1)+1/2}_{\alpha,i}, \tag{3.5}$$

where

$$\Theta^{n}_{\alpha,i} = \frac{f^{n,j}_{\alpha,i} - f^{n,j}_{\alpha,i-1}}{f^{n,j}_{\alpha,i+1} - f^{n,j}_{\alpha,i}}, \tag{3.6}$$

$$\Theta^{n,j}_{\alpha} = \frac{f^{n,j}_{\alpha,i} - f^{n,j-1}_{\alpha,i}}{f^{n,j+1}_{\alpha,i} - f^{n,j}_{\alpha,i}}, \tag{3.7}$$

and the minmod flux limiter is given by

$$\Psi\left(\Theta\right) = \max\left[0, \min(1, \Theta)\right]. \tag{3.8}$$

For simplicity, only the formulae for $c_{\alpha y} > 0$ and $c_{\alpha x} > 0$ are given.

3.2. *Boundary condition*

Gas-wall interactions are captured by boundary conditions. The most popular boundary condition is the Maxwell model (Cercignani 2000; Clerk Maxwell 1879), in which a fraction $(1 - \gamma)$ of gas particles are assumed to undergo specular reflection while the remaining particles are diffusely reflected. In the limit of $\gamma = 1$, the reflection becomes fully diffuse.

As lattice models are derived from continuous kinetic equations, their boundary conditions may be obtained from the continuous kinetic theory (Ansumali & Karlin 2002). It has already been shown that lattice models with diffuse type wall boundary can describe a range of rarefied effects (see, e.g., Meng & Zhang 2011*b*; Kim *et al.* 2008*a*; Yudistiawan *et al.* 2008). In this work, our primary interest is the model accuracy; as a result we will only implement the Maxwellian diffuse wall boundary.

The boundary condition employed in this work is Version 1 of boundary conditions

in Sofonea (2009), which is briefly described below. Firstly, the truncated Maxwellian distribution function can be written as

$$\begin{aligned} f_\alpha^0 &= \rho S(T, \boldsymbol{u}) \\ &= \rho w_\alpha \Big\{ 1 + c_i u_i + \frac{1}{2}\left[(c_i u_i)^2 - u_i u_i + (T-1)(c_i c_i - D)\right] \\ &+ \frac{c_i u_i}{6}[(c_i u_i)^2 - 3u_i u_i + 3(T-1)(c_i c_i - D - 2)] \\ &+ \frac{1}{24}[(c_i u_i)^4 - 6(u_i c_i)^2 u_j u_j + 3(u_j u_j)^2] \\ &+ \frac{T-1}{4}[(c_i c_i - D - 2)((u_i c_i)^2 - u_i u_i) - 2(u_i c_i)^2] \\ &+ \frac{(T-1)^2}{8}\left[(c_i c_i)^2 - 2(D+2)c_i c_i + D(D+2)\right] \Big\}. \end{aligned} \tag{3.9}$$

As the discretization is conducted along a Cartesian coordinate system (see Fig.2), the wall boundary condition can be written as

$$f_{\alpha,k}^0 = \rho_{W,k} S(T_{W,k}, \boldsymbol{u}_{W,k}) \quad \boldsymbol{\xi}_\alpha \cdot \boldsymbol{n} > 0, \tag{3.10}$$

where

$$\rho_{W,k} = \frac{\sum\limits_{(\boldsymbol{\xi}_\alpha \cdot \boldsymbol{n}) < 0} |\boldsymbol{\xi}_\alpha \cdot \boldsymbol{n}|\, f_{\alpha,k}^1}{\sum\limits_{(\boldsymbol{\xi}_\alpha \cdot \boldsymbol{n}) > 0} |\boldsymbol{\xi}_\alpha \cdot \boldsymbol{n}|\, S(T_{W,k}, \boldsymbol{u}_{W,k})}, \tag{3.11}$$

Here, subscript W denotes the computational nodes at the wall, $\rho_{W,k}$ is the density on the wall nodes k (see Fig.2), $T_{W,k}$ is the temperature, $\boldsymbol{u}_{W,k}$ the velocity and $\boldsymbol{n}$ the inward unit vector normal to the wall. The distribution function at the ghost nodes is assumed to be identical to those on the corresponding wall nodes.

4. Validation

We have validated the proposed scheme using a variety of flows, both in the low-Mach and high-Mach number limit. Unless otherwise stated, our rsults have been obtained using a 11th-order of discrete velocity set, which represents a good compromise between accuracy (expected to be accurate at the Burnett level, see Sec.2.3) and computational efficiency. Our numerical results will be compared with DSMC and LVDSMC (see Homolle & Hadjiconstantinou 2007; Radtke & Hadjiconstantinou 2009, 2011) simulations, while in some cases, numerical solutions of the ES-BGK equation and the R13 model will also be presented.

The flows considered here are one-dimensional and are confined by two infinite parallel plates in the $x - z$ plane. The distance between the two plates (in the y direction) is L on which the Knudsen number

$$K_D = \sqrt{\frac{\pi}{2}} Kn \tag{4.1}$$

is based. Comparisons with the hard-sphere gas will be performed by setting the Prandtl number to 2/3, i.e. $b = -1/2$. For the BGK gas, the Prandtl number is unity which corresponds to $b = 0$. Furthermore, the gas has the heat capacity $C_p = 5/2$, i.e., the spatial dimension D is set to be 3, see Eqs. (2.3) and (3.9). Our 3D simulation results are described below.

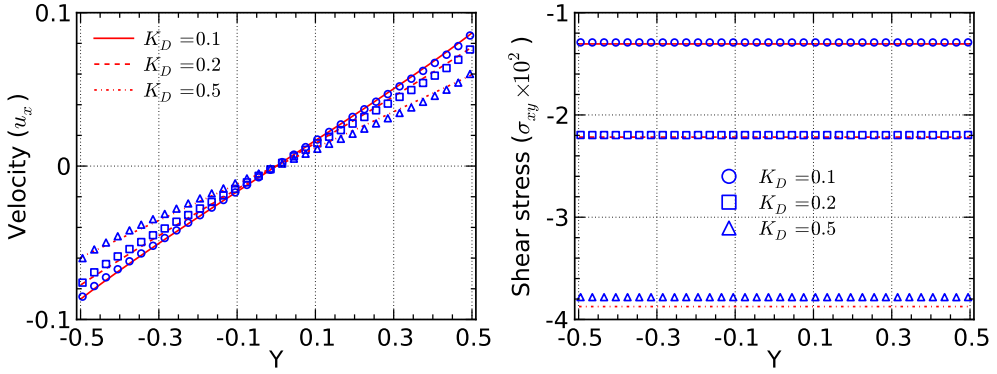

FIGURE 3. The velocity and shear stress profiles for Couette flow of a hard-sphere gas at $K_D = 0.1$, 0.2 and 0.5. The symbols denote DSMC data and the lines represent the lattice ES-BGK results. The wall velocities are $u_w = \pm 0.1$.

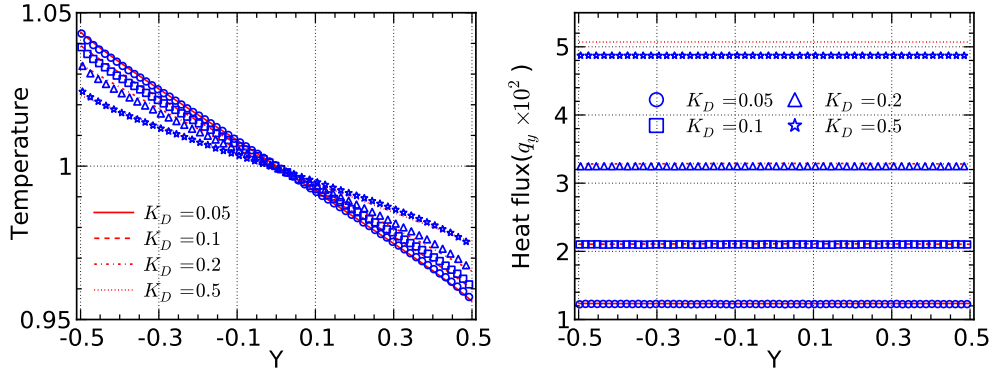

FIGURE 4. The temperature and heat flux profiles for a Fourier problem for a hard-sphere gas at $K_D = 0.05, 0.1$, 0.2 and 0.5 with the wall temperature difference 0.1. The symbols denote DSMC data and the lines represent the lattice ES-BGK results.

4.1. *Low Mach number flows*

Flows in the low-Mach number limit are of particular interest since they are most often encountered in micro/nanofluidic applications (Cercignani 2006; Hadjiconstantinou 2006). Here we provide validation of our methodology using traditional Couette and Fourier flows. We also present solutions of an unsteady boundary heating problem that features coupled momentum and heat transfer and thus requires an accurate representation of the ratio of the associated transport coefficients, namely the Prandtl number. This problem also allows us to investigate the limitations of the proposed model in the presence of kinetic effects due to flow unsteadiness.

4.1.1. *Steady Couette and Fourier Flows*

Figures 3 and 4 show comparison between our lattice results and DSMC simulations for a Couette and a Fourier heat tranfer problem respectively. In the Couette flows, the walls move with velocities $u_w = \pm 0.1$, while in the Fourier problems the wall temperatures are $T_w = 1 \pm 0.05$. Fig. 4 shows that the proposed lattice ES-BGK model can be used to approximate the hard-sphere gas thermal conductivity by setting the Prandtl number to 2/3. Both figures show that the agreement in the slip-flow regime is excellent; as K_D increases into the transition regime, a small amout of error is evident. This error increases

further as K_D increases, but remains very reasonable for $K_D < 0.5$; for example, for both flows, at $K_D = 0.5$ the error is less than 5%.

4.2. *Unsteady boundary heating problems*

In this section we present results from an unsteady boundary heating problem of the kind studied in (Manela & Hadjiconstantinou 2007); these studies are motivated by the common occurrence of applications involving time-varying boundary temperatures in micro-electro-mechanical devices. In this problem, the two walls confining the gas are heated uniformly via prescribed time dependent temperatures of the form $T_w = 1 + F(t)$. Here, $F(t)$ is taken to be a sinusoidal function $\sin(\theta t)$ with an amplitude (0.002 in simulations) that is sufficiently small to justify a linear assumption. As this is a time-varying problem, another non-dimensional parameter needs to be introduced (Manela & Hadjiconstantinou 2008, 2010), namely the Strouhal number, defined as

$$St = \theta = \frac{\hat{\theta} L}{\sqrt{R T_0}}. \tag{4.2}$$

Kinetic effects become important as both the Strouhal and Knudsen numbers increase as shown in Fig. 6 in Manela & Hadjiconstantinou (2010).

Here, simulations will be conducted for a range of Strouhal and Knudsen numbers. Prandtl numbers corresponding both to the hard-sphere and BGK model will be considered. The accuracy of the lattice results will be evaluated by comparison with simulation results obtained using the recently developed low-variance deviational simulation Monte Carlo (LVDSMC) method (Homolle & Hadjiconstantinou 2007; Radtke & Hadjiconstantinou 2009, 2011) because simulation of this low-Mach number flow by DSMC is prohibitively expensive. The LVDSMC method was developed to specifically address this DSMC limitation, namely the prohibitive computational cost associated with low-Ma and more generally low-signal flows. LVDSMC provides efficient numerical solutions of the Boltzmann equation for all Knudsen numbers (Wagner 2008) and *arbitrarily small signals* by simulating only the deviation from equilibrium. This control-variate variance-reduction formulation introduces deterministic knowledge of a nearby equilibrium state, and thus significantly reduces the stastistical uncertainty associated with the Monte Carlo approach *without introducing any approximation*. The resulting computational benefits in the limit of low speed flows such as the one considered here are typically very large (Homolle & Hadjiconstantinou 2007).

Following Manela & Hadjiconstantinou (2010), comparison with LVDSMC results will be performed using the following two Knudsen numbers:

$$K_E = \frac{16}{5\sqrt{2\pi}} Kn, \tag{4.3}$$

for the hard-sphere gas with $Pr = 2/3$, and

$$K_B = \sqrt{\frac{8}{\pi}} Kn \tag{4.4}$$

for the BGK gas with $Pr = 1$. Details on the LVDSMC simulations of the problem studied here can be found in Manela & Hadjiconstantinou (2008, 2010).

The results for various Strouhal and Knudsen numbers for the hard-sphere and the presented in Figs.5-8, where both the velocity u_y and temperature perturbation $\Delta T = T - 1$ are normalized by the amplitude of $F(t)$. Figs.9-12 show results for the BGK model. Symbols denote the lattice model proposed here, whereas lines denote LVDSMC data. At $St = \pi\sqrt{2}/16$, the two sets of results show good agreement, even when $K_E = 0.5$

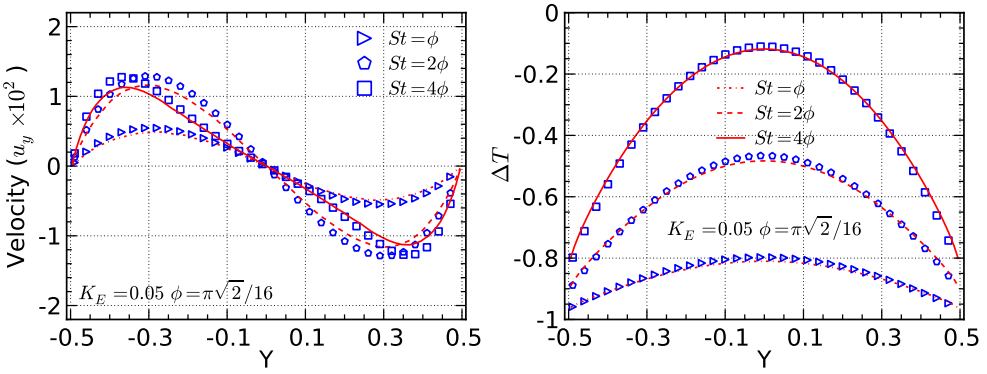

FIGURE 5. The velocity and temperature perturbations for a hard-sphere gas subject to a sinusoidal heating at $t = 3\pi/2$ at different Kn and St. The symbols correspond to the data of the lattice model ($Pr = 2/3$) and the lines are the results of the LVDSMC method.

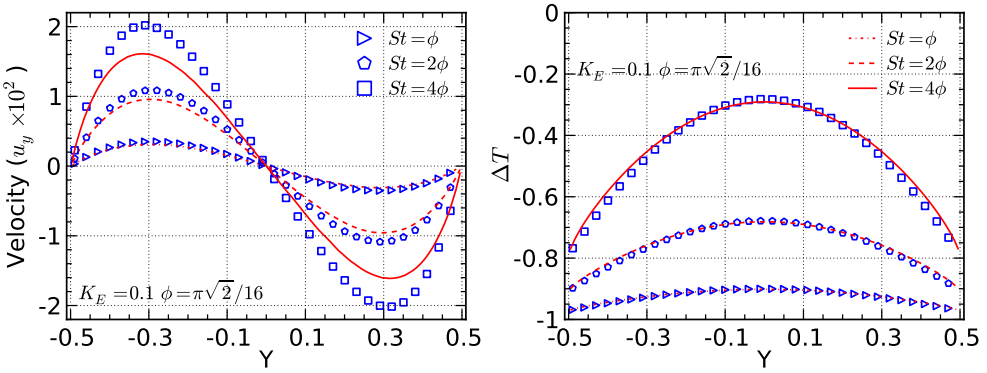

FIGURE 6. The velocity and temperature perturbations (ΔT) for a hardsphere gas subject to a sinusoidal heating at $t = 3\pi/2$ at different Kn and St. The symbols correspond to the data of the lattice model ($Pr = 2/3$) and the lines are the results of the LVDSMC method.

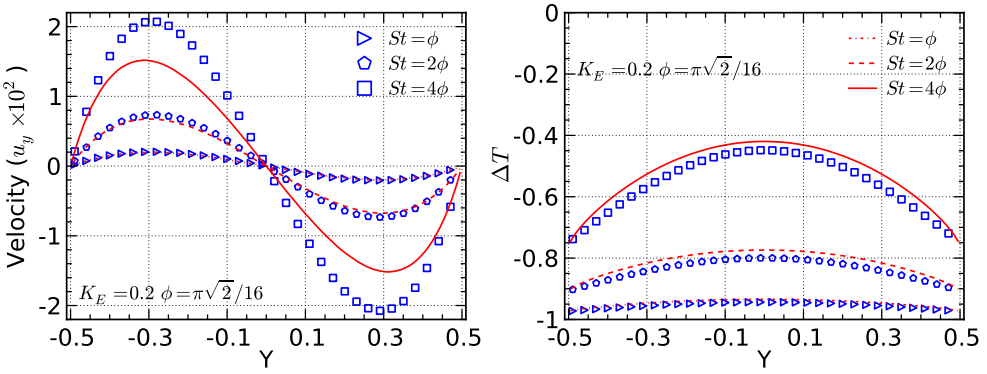

FIGURE 7. The velocity and temperature perturbations for a hard-sphere gas subject to a sinusoidal heating at $t = 3\pi/2$ at different Kn and St. The symbols correspond to the data of the lattice model ($Pr = 2/3$) and the lines are the results of the LVDSMC method.

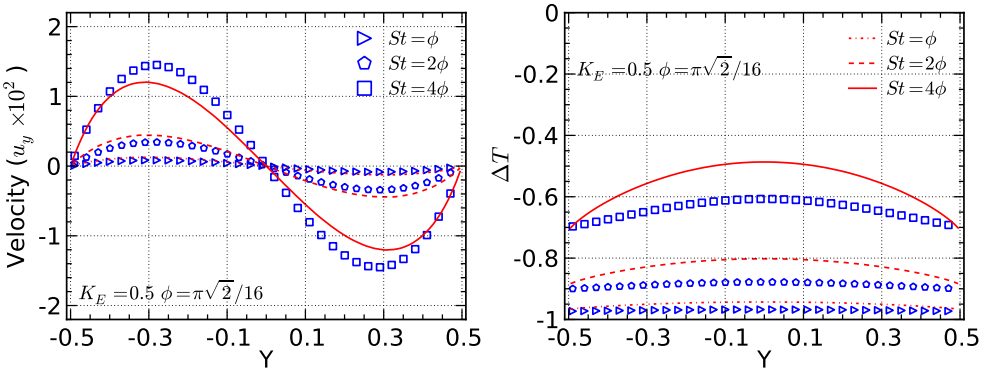

FIGURE 8. The velocity and temperature perturbations for a hard-sphere gas subject to a sinusoidal heating at $t = 3\pi/2$ at different Kn and St. The symbols correspond to the data of the lattice model ($Pr = 2/3$) and the lines are the results of the LVDSMC method.

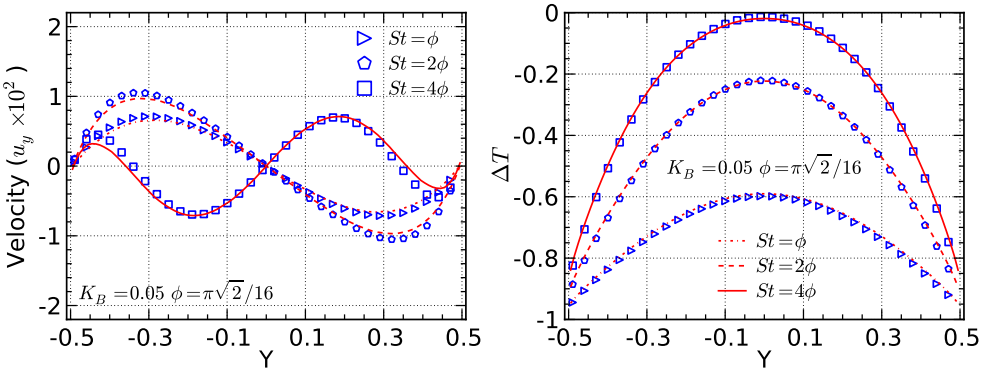

FIGURE 9. The velocity and temperature perturbations for a BGK gas subject to a sinusoidal heating at $t = 3\pi/2$ at different Kn and St. The symbols correspond to the data of the lattice model ($Pr = 1$) and the lines are the results of the LVDSMC method.

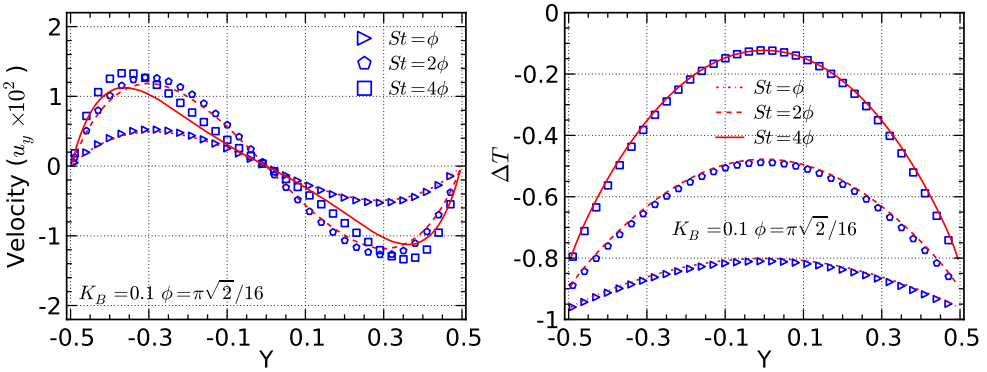

FIGURE 10. The velocity and temperature perturbations (ΔT) for a BGK gas subject to a sinusoidal heating at $t = 3\pi/2$ at different Kn and St. The symbols correspond to the data of the lattice model ($Pr = 1$) and the lines are the results of the LVDSMC method.

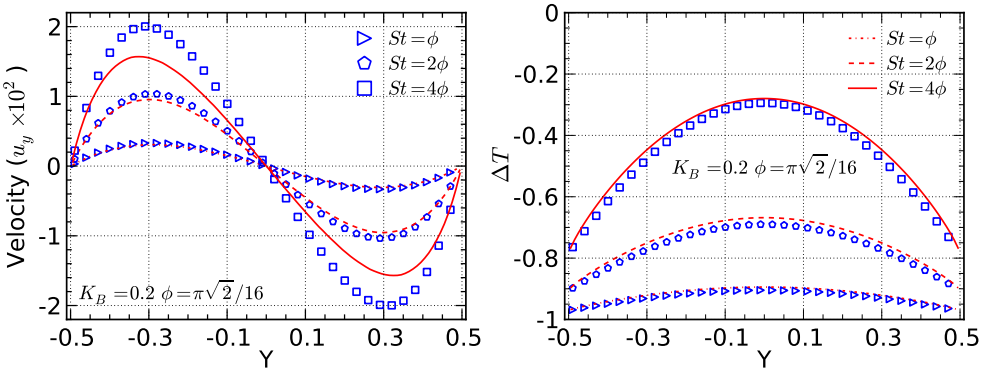

FIGURE 11. The velocity and temperature perturbations for a BGK gas subject to a sinusoidal heating at $t = 3\pi/2$ at different Kn and St. The symbols correspond to the data of the lattice model ($Pr = 1$) and the lines are the results of the LVDSMC method.

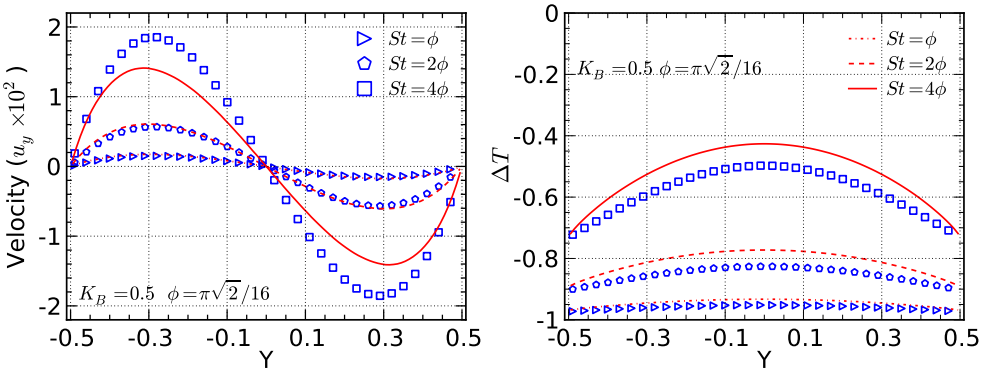

FIGURE 12. The velocity and temperature perturbations for a BGK gas subject to a sinusoidal heating at $t = 3\pi/2$ at different Kn and St. The symbols correspond to the data of the lattice model ($Pr = 1$) and the lines are the results of the LVDSMC methods.

or $K_B = 0.5$. With increasing Strouhal number, disprepancies between the two appear and become larger. For $St = \pi\sqrt{2}/4$, significant disagreement is observed even for K_E as low as 0.05. Larger Strouhal numbers lead to stronger rarefaction effects, so this disagreement can be attributed to the moderate discrete velocity set. Overall, with this moderate discrete velocity set, the present model can give reasonable predictions for flows with a Knudsen number up to 0.5 and a Strouhal number up to $\pi\sqrt{2}/8$. If highly accurate results are desirable, more discrete velocities are required, leading to higher computational costs.

4.3. *High-Mach number flows*

In this section we present simulation results for high Mach number flows such as Couette flows with $u_w \pm 0.2$ and forced Poiseuille flows with non-dimensional forcing magnitude $g = 0.22$. Although in the Couette flows the wall speed is only a factor of 2 larger than the flows examined in section 4.1, our focus here turns to the resulting temperature field that, despite the small temperature differences involved, reveals useful information.

Fig. 13 shows a comparison between our lattice model, DSMC and numerical solution of the ES-BGK equation for a Couette flow at $K_D = 0.05$. The comparison reveals that at these small K_D, the lattice model can capture both kinetic (e.g. slip/temperature jump) and non-equilibrium effects quite accurately. For comparison, the results of the BGK

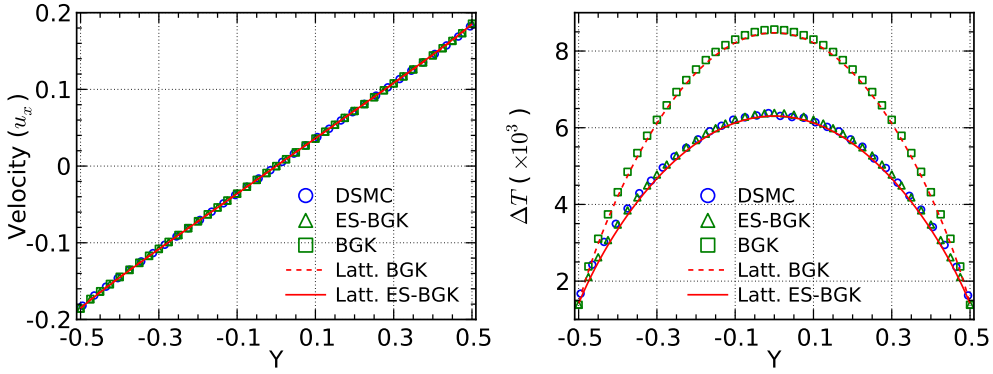

FIGURE 13. The velocity and temperature profiles for the Couette flow at $K_D = 0.05$, where $\Delta T = T - T_w$. The wall velocities are $u_w = \pm 0.2$.

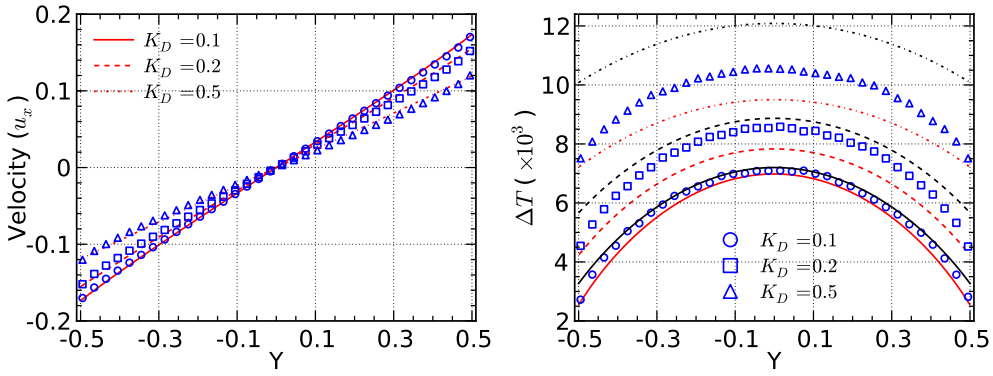

FIGURE 14. The velocity and temperature profiles ($\Delta T = T - T_w$) for Couette flow of a hard–sphere gas at $K_D = 0.1$, 0.2 and 0.5. The symbols denote the DSMC data and the red lines represent the lattice ES-BGK results. The wall velocities are $u_w = \pm 0.2$. For further comparison, the temperature profiles predicted by the R13 model (Taheri *et al.* 2009) are also presented with the black lines where the line styles same to those of the lattice ES-BGK results are used to distinguish the Knudsen numbers.

equation and its lattice version ($b = 0$) are also presented. These two models predict a temperature maximum that is 30% higher than the hard-sphere result.

Results for Couette flows in the transition regime are presented in Figs. 14 and 15. Overall, our model predictions for the velocity, shear stress and heat flux are close to those of DSMC even for $K_D = 0.5$. However, our predictions of the viscous-heating-induced temperature field start to deviate from the DSMC results at $K_D = 0.2$. Remarkably, the heat flux predictions of the lattice model are still in excellent agreement with the DSMC data for K_D as large as 0.5.

To further validate the model accuracy beyond the NS level, the profiles of shear stress σ_{yy} and stream-wise heat flux q_x are presented in Fig.(16), which are both zero for the NS solutions. However, our lattice model can give reasonable predictions for σ_{yy} up to $K_D = 0.2$ which is consistent with the temperature prediction. For the heat flux q_x, we have similar observation, which further confirms that our model can describe kinetic effects beyond the NS level with the chosen moderate 11-th order quadrature, which is consistent with the discussion in Sec.2.3. It is also interesting to compare with the predictions of the R13 model, which gives a stable set of transport equations of the

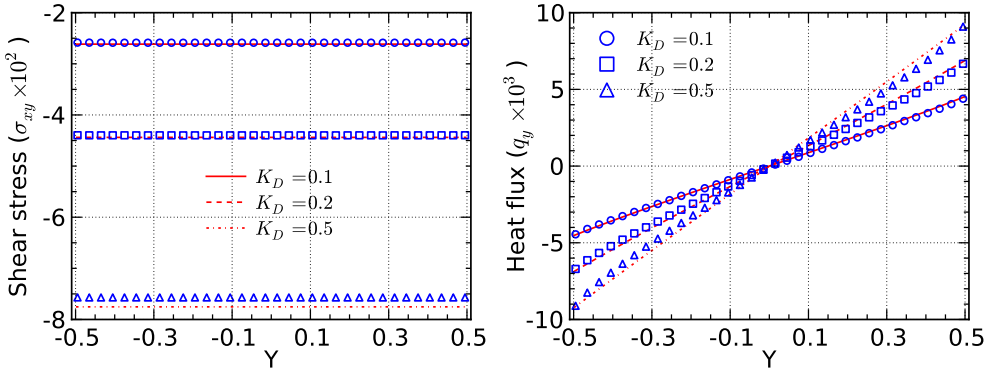

FIGURE 15. The shear stress σ_{xy} and heat flux q_y profiles for Couette flow of a hard-sphere gas at $K_D = 0.1$, 0.2 and 0.5. The symbols denote DSMC data and the lines represent the lattice ES-BGK results. The wall velocities are $u_w = \pm 0.2$.

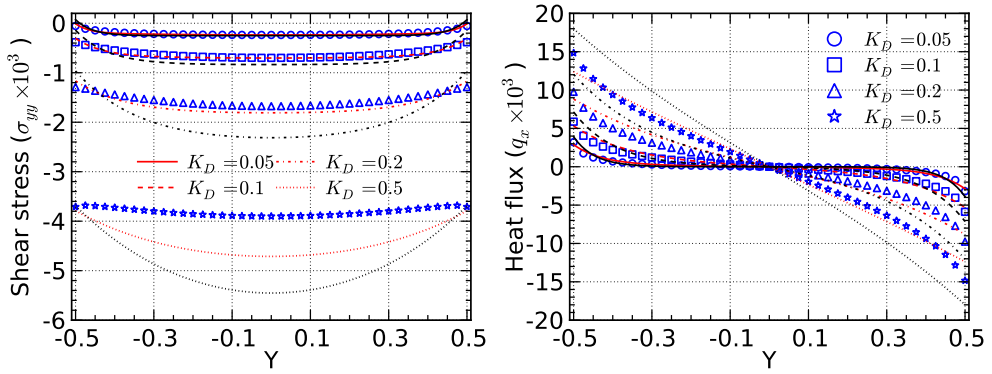

FIGURE 16. The shear stress σ_{yy} and heat flux q_x profiles for Couette flow of a hard-sphere gas at $K_D = 0.1$, 0.2 and 0.5. The symbols denote direct solution of the ES-BGK equation, the red lines represent the lattice ES-BGK results and the black lines are those of the R13 model(Taheri *et al.* 2009). The Knudsen numbers for the R13 model are also distinguished by the line styles same to those of the lattice ES-BGK results. The wall velocities are $u_w = \pm 0.2$.

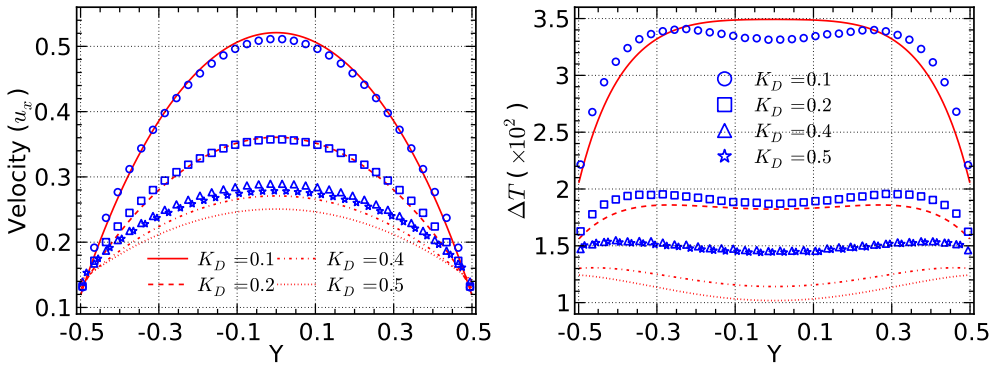

FIGURE 17. The velocity and temperature profiles ($\Delta T = T - T_w$) for the force-driven Poiseuille flow of a hard-sphere gas at $K_D = 0.1$, 0.2, 0.4 and 0.5. The symbols denote DSMC data and the lines represent the lattice ES-BGK results.

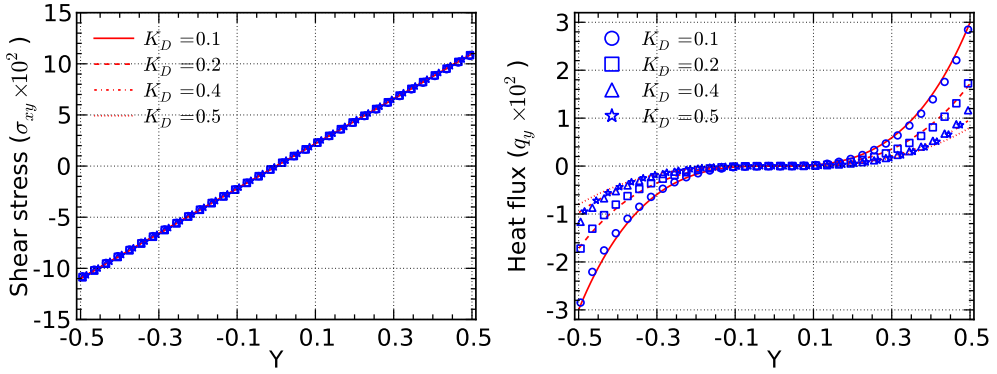

FIGURE 18. The shear stress and heat flux profiles for the force-driven Poiseuille flow of a hard-sphere gas at $K_D = 0.1$, 0.2, 0.4 and 0.5. The symbols denote DSMC data and the lines represent the lattice ES-BGK results.

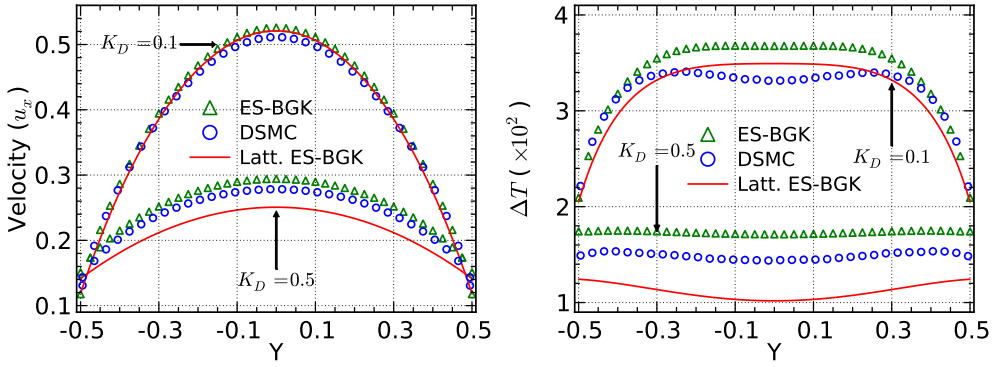

FIGURE 19. Comparisons of the velocity and temperature profiles ($\Delta T = T - T_w$) for the force-driven flow among the ES-BGK equation, lattice ES-BGK model and DSMC method at $K_D = 0.1$ and 0.5.

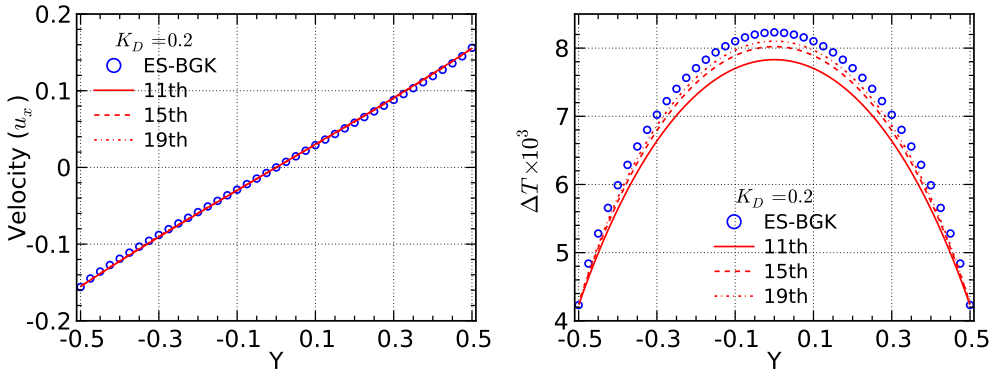

FIGURE 20. Convergence comparison for a Couette flow at $K_D = 0.2$ with wall velocities $u_w = \pm 0.2$. Lines denote the lattice model data, and the adopted discrete velocity order as denoted in the legend. Improved accuracy is observed as the number of discrete velocities is increased.

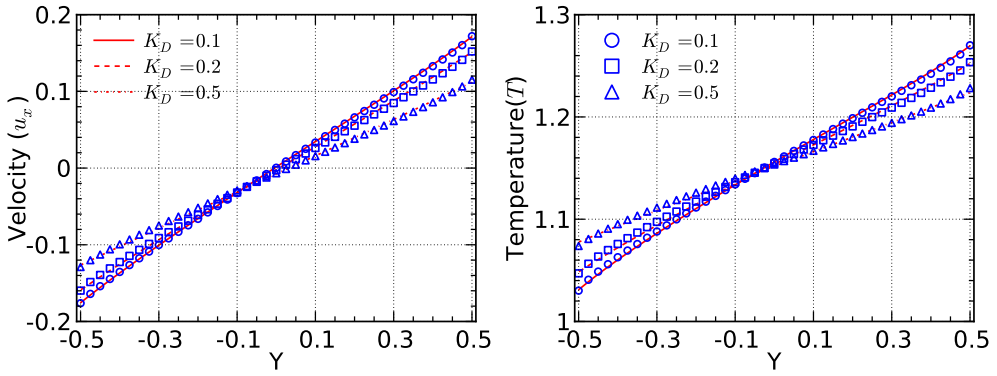

FIGURE 21. Comparisons of the velocity and temperature profiles for the combined Couette–Fourier flows. The wall velocities are $u_w = \pm 0.2$ while the wall temperature difference is 0.3. The lines are the lattice ES-BGK model data and the symbols are the results of the ES-BGK equation.

super-Burnett order (Taheri *et al.* 2009). Fig.(16) shows similar performance for both of the R13 model and our lattice model.

The simulation results for Poiseuille flows at four Knudsen numbers are depicted in Figs. 17 and 18. This flow is more numerically challenging compared to the Couette flow. Even for K_D as small as 0.1, the temperature profiles show significant difference between the lattice model and DSMC results, even though the bimodal temperature distribution (Mansour *et al.* 1997) can be qualitatively captured by the lattice model at $K_D = 0.2$. As the Knudsen number increases further, the difference becomes even larger, though the temperature minimum at the center of the computational domain can be predicted qualitatively. Remarkably, but also consistently with the Couette flow case, the heat flux profiles show good agreement with the DSMC data despite the more significant discrepancies in the temperature profiles.

The inability of our model to predict accurate viscous heating may be caused by two factors. First, as shown in the derivation process, the lattice model approaches the corresponding kinetic model via the moment representation with increasing order of Gauss-Hermite quadrature. However, as discussed in Sec.2.3, the chosen moderate discrete velocity set is only expected to approach the Burnett level, which may not be sufficient to capture all kinetic effects in the presence of a non-negligible Mach number. This is verified in Fig. 20 where its is shown that increasing discrete velocities can improve the model accuracy.

In addition to the error due to a finite number of discrete velocities, the ES-BGK equation itself is a model which may be failing in these flows. In fact, as shown by some studies (e.g., Gallis & Torczynski 2011), the ES-BGK equation tends to produce inaccurate velocity distribution functions. The possibility that the ES-BGK model is itself contributing to the error can be confirmed by the results presented in Fig. 19. At $K_D = 0.5$ the lattice model result shows a significant deviation from the numerical solution of the ES-BGK model. Meanwhile, the temperature profile from numerical solution of the ES-BGK equation itself shows a large deviation from the DSMC result.

While the comparisons with the DSMC solutions for the temperature difference of 0.1 have been shown in Fig. 4, a larger temperature difference of 0.3 is investigated for the combined Couette-Fourier flow. The results are shown in Fig. 21 where excellent agreement is observed between the lattice ES-BGK model and the ES-BGK equation.

5. Concluding remarks

We have presented and validated a lattice Boltzmann model using a systematic Hermite moment representation of the ES-BGK equation. The resulting lattice ES-BGK model features an adjustable Prandtl number and may thus be more appropriate for use in coupled thermofluidic phenomena. This generic procedure may be applied to other kinetic model equations.

We have validated the lattice model for combined thermal and rarefaction effects by comparing its predictions with the DSMC and LVDSMC results as well as numerical solutions of the ES-BGK model. We find that, for a moderate 11th-order discrete velocity set, the proposed model can provide reasonable predictions for Couette and force-driven Poiseuille flows for Knudsen numbers up to 0.5. In addition, it is able to accurately predict heat conduction in the slip-flow and early transition regimes. This finding extends to unsteady problems provided the additional kinetic effects due to their time-dependence are also considered: for an unsteady boundary heating problem reasonable agreement with LVDSMC simulations is observed for Knudsen numbers up to 0.5 and Strouhal numbers up to $\pi\sqrt{2}/8$.

The solutions obtained by the lattice Boltzmann method are expected to approach the "true" solutions of the ES-BGK equation as the number of discrete velocities and the Hermite expansion order is increased. However, the moderate discrete velocity set used here already represents a reasonable compromise between computational efficiency and modeling accuracy for flows with a range of Knudsen and Strouhal numbers. Although we have tested the model for rarefied gas thermal flows, this model, in principle, can be used for liquid thermal flows, which will be the subject of future work.

REFERENCES

Andries, Pierre, Bourgat, Jean-François, le Tallec, Patrick & Perthame, Benoit 2002 Numerical comparison between the Boltzmann and ES-BGK models for rarefied gases. *Comput. Methods Appl. Mech. Engrg.* **191** (31), 3369–3390.

Andries, Pierre, Tallec, Patrick Le, Perlat, Jean-Philippe & Perthame, Benoît 2000 The Gaussian-BGK model of Boltzmann equation with small Prandtl numbe. *Eur. J. Mech. B - Fluids* **19** (6), 813–830.

Ansumali, S., Karlin, I. V., Arcidiacono, S., Abbas, A. & Prasianakis, N. I. 2007 Hydrodynamics beyond Navier-Stokes: Exact Solution to the lattice Boltzmann hierarchy. *Phys. Rev. Lett.* **98** (12), 124502.

Ansumali, Santosh & Karlin, Iliya V. 2002 Kinetic boundary conditions in the lattice Boltzmann method. *Phys. Rev. E* **66** (2), 26311.

Aoki, Kazuo, Takata, Shigeru & Nakanishi, Toshiyuki 2002 Poiseuille-type flow of a rarefied gas between two parallel plates driven by a uniform external force. *Phys. Rev. E* **65** (2), 26315.

Cercignani, Carlo 2000 *Rarefied Gas Dynamics: From Basic Concepts to Actual Calculations*. Cambridge University Press.

Cercignani Carlo 2006 Slow rarefied flows: Theory and application to Micro-Electro-Mechanical systems. Birkhauser.

Chen, S. Y. & Doolen, G. D. 1998 Lattice Boltzmann method for fluid flows. *Annu. Rev. Fluid Mech.* **30**, 329–364.

Chikatamarla, Shyam S. & Karlin, Iliya V. 2006 Entropy and Galilean invariance of lattice Boltzmann theories. *Phys. Rev. Lett.* **97** (19), 190601.

Chikatamarla, Shyam S. & Karlin, Iliya V. 2009 Lattices for the lattice Boltzmann method. *Phys. Rev. E* **79** (4), 46701.

Clerk Maxwell, J. 1879 On stresses in rarified gases arising from inequalities of temperature. *Phil. Trans. R. Soc. Lond.* **170**, 231–256.

Gallis, M. A. & Torczynski, J. R. 2011 Investigation of the ellipsoidal-statistical Bhatnagar-

Gross-Brook kinetic model applied to gas-phase transport of heat and tangential momentum between parallel walls. *Phys. Fluids* **23** (3), 030601.

Garzó, Vicente & Andrés Santos 1995 Comparison between the Boltzmann and BGK equations for uniform shear flow. *Physica A* **213**, 426–434.

Gonnella, G., Lamura, A. & Sofonea, V. 2007 Lattice Boltzmann simulation of thermal nonideal fluids. *Phys. Rev. E* **76** (3), 36703.

Graur, Irina & Polikarpov, A. 2009 Comparison of different kinetic models for the heat transfer problem. *Heat and Mass Transfer* **46** (2), 237–244.

Grad, H 1949 On the kinetic theory of rarefied gases. *Commun. Pure Appl. Math.* **2**, 331–407.

Grad, H 1958 *Principles of the Kinetic Theory of Gases*, Handbuch der Physik XII: Thermodynamik der gase edn. Berlin: Springer.

Gu, X J & Emerson, D R 2007 A computational strategy for the regularized 13 moment equations with enhanced wall-boundary conditions. *J. Comput. Phys.* **225** (1), 263–283.

Gu, Xiao-jun & Emerson, David R 2009 A high-order moment approach for capturing non-equilibrium phenomena in the transition regime. *J. Fluid Mech.* **636** (-1), 177–216.

Guo, Zhaoli, Zheng, Chuguang, Shi, Baochang & Zhao, T. S. 2007 Thermal lattice Boltzmann equation for low Mach number flows: Decoupling model. *Phys. Rev. E* **75** (3), 36704.

Guo, ZhaoLi, Zhao, T. S. & Shi, Yong 2006 Physical symmetry, spatial accuracy, and relaxation time of the lattice Boltzmann equation for microgas flows. *J. Appl. Phys.* **99** (7), 74903.

Hadjiconstantinou, Nicolas G. 2006 The limits of Navier-Stokes theory and kinetic extensions for describing small–scale gaseous hydrodynamics. *Phys. Fluids* **18** (11), 111301.

Han, Yen-lin, Muntz, Eric Phillip & Alexeenko, Alina 2011 Nanoscale and microscale thermophysical engineering experimental and computational studies of temperature gradient–driven molecular transport in gas flows through nano / microscale Channels. *Nanoscale Microscale Thermophys. Eng.* pp. 37–41.

Han, Yen-Lin, Phillip Muntz, Eric, Alexeenko, Alina & Young, Marcus 2007 Experimental and computational studies of temperature gradient-driven molecular transport in gas flows through nano/microscale channels. *Nanoscale Microscale Thermophys. Eng.* **11** (1-2), 151–175.

He, Xiaoyi, Chen, Shiyi & Doolen, Gary D 1998 A novel thermal model for the lattice Boltzmann method in incompressible limit. *J. Comput. Phys.* **146** (1), 282–300.

Holway, Lowell H 1966 New statistical models for kinetic theory: Methods of construction. *Phys. Fluids* **9** (9), 1658–1673.

Homolle, Thomas M. M. & Hadjiconstantinou, Nicolas G. 2007 A low-variance deviational simulation Monte Carlo for the Boltzmann equation. *J. Comput. Phys.* **226** (2), 2341–2358.

Kim, Seung Hyun, Pitsch, Heinz & Boyd, Iain D. 2008*a* Accuracy of higher-order lattice Boltzmann methods for microscale flows with finite Knudsen numbers. *J. Comput. Phys.* **227** (19), 8655–8671.

Kim, Seung Hyun, Pitsch, Heinz & Boyd, Iain D. 2008*b* Slip velocity and Knudsen layer in the lattice Boltzmann method for microscale flows. *Phys. Rev. E* **77** (4), 26704.

Lallemand, Pierre & Luo, Li-Shi 2003 Theory of the lattice Boltzmann method: Acoustic and thermal properties in two and three dimensions. *Phys. Rev. E* **68** (3), 36706.

Manela, A. & Hadjiconstantinou, N. G. 2007 On the motion induced in a gas confined in a small-scale gap due to instantaneous heating. *J. Fluid Mech.* **593**, 453–462.

Manela, Avshalom & Hadjiconstantinou, Nicolas G. 2008 Gas motion induced by unsteady boundary heating in a small-scale slab. *Phys. Fluids* **20** (11), 117104.

Manela, A & Hadjiconstantinou, N. G. 2010 Gas-flow animation by unsteady heating in a microchannel. *Phys. Fluids* **22** (6), 62001.

Mansour, M. Malek, Baras, F. & Garcia, Alejandro L. 1997 On the validity of hydrodynamics in plane Poiseuille flows. *Physica A* **240** (1-2), 255–267.

Meng, Jianping & Zhang, Yonghao 2011*a* Accuracy analysis of high-order lattice Boltzmann models for rarefied gas flows. *J. Comput. Phys.* **230** (3), 835–849.

Meng, Jianping & Zhang, Yonghao 2011*b* Gauss-Hermite quadratures and accuracy of lattice Boltzmann models for nonequilibrium gas flows. *Phys. Rev. E* **83** (3).

Mieussens, Luc & Struchtrup, Henning 2004 Numerical comparison of Bhatnagar–Gross–Krook models with proper Prandtl number. *Phys. Fluids* **16** (8), 2797–2813.

Prasianakis, Nikolaos I. & Karlin, Iliya V. 2007 Lattice Boltzmann method for thermal flow simulation on standard lattices. *Phys. Rev. E* **76** (1), 16702.

Prasianakis, Nikolaos I. & Karlin, Iliya V. 2008 Lattice Boltzmann method for simulation of compressible flows on standard lattices. *Phys. Rev. E* **78** (1), 16704.

Prasianakis, N. I., Karlin, I. V., Mantzaras, J. & Boulouchos, K. B. 2009 Lattice Boltzmann method with restored Galilean invariance. *Phys. Rev. E* **79** (6), 66702.

Radtke, Gregg A. & Hadjiconstantinou, Nicolas G. 2009 Variance-reduced particle simulation of the Boltzmann transport equation in the relaxation-time approximation. *Phys. Rev. E* **79** (5), 56711.

Radtke, Gregg A., Hadjiconstantinou, Nicolas G. & Wagner Wolfgang 2011 Low-noise Monte Carlo simulation of the variable hard-sphere gas. *Phys. Fluids*, **23**, 030606.

Sbragaglia, M., Benzi, R., Biferale, L., Chen, H., Shan, X. & Succi, S. 2009 Lattice Boltzmann method with self-consistent thermo-hydrodynamic equilibria. *J. Fluid Mech.* **628**, 299–309.

Sbragaglia, M. & Succi, S. 2005 Analytical calculation of slip flow in lattice Boltzmann models with kinetic boundary conditions. *Phys. Fluids* **17** (9), 93602.

Sbragaglia, M. & Succi, S. 2006 A note on the lattice Boltzmann method beyond the Chapman-Enskog limits. *Europhys. Lett.* **73** (3), 370–376.

Scagliarini, A., Biferale, L., Sbragaglia, M., Sugiyama, K. & Toschi, F 2010 Lattice Boltzmann methods for thermal flows: Continuum limit and applications to compressible Rayleigh–Taylor systems. *Phys. Fluids* **22** (5), 55101.

Shan, Xiaowen 1997 Simulation of Rayleigh-Bénard convection using a lattice Boltzmann method. *Phys. Rev. E* **55** (3), 2780–2788.

Shan, Xiao Wen & He, Xiao Yi 1998 Discretization of the velocity space in the solution of the Boltzmann equation. *Phys. Rev. Lett.* **80** (1), 65–68.

Shan, Xiaowen 2010 General solution of lattices for Cartesian lattice Bhatanagar-Gross-Krook models. *Phys. Rev. E* **81** (3), 36702.

Shan, X. & Chen, H. 2007 A general multiple-relaxation Boltzmann collision model. *Int. J. Mod. Phys. C* **18**, 635–643.

Shan, X. W., Yuan, X. F. & Chen, H. D. 2006 Kinetic theory representation of hydrodynamics: A way beyond the Navier Stokes equation. *J. Fluid Mech.* **550**, 413–441.

Shim, Jae & Gatignol, Renée 2011 Thermal lattice Boltzmann method based on a theoretically simple derivation of the Taylor expansion. *Phys. Rev. E* **83** (4), 2–6.

Sofonea, Victor 2009 Implementation of diffuse reflection boundary conditions in a thermal lattice Boltzmann model with flux limiters. *J. Comput. Phys.* **228** (17), 6107–6118.

Struchtrup, Henning 2004 Stable transport equations for rarefied gases at high orders in the knudsen number. *Phys. Fluids* **16** (11), 3921–3934.

Struchtrup, H. 2005 Derivation of 13 moment equations for rarefied gas flow to second order accuracy for arbitrary interaction potentials. *Multiscale Model.Simul.* **3** (1), 221–243.

Struchtrup, Henning 2005*b* *Macroscopic Transport Equations for Rarefied Gas Flows*. Springer Berlin / Heidelberg.

Struchtrup, Henning & Torrilhon, Manuel 2003 Regularization of Grad's 13 moment equations: Derivation and linear analysis. *Phys. Fluids* **15** (9), 2668–2680.

Succi, Sauro 2002 Mesoscopic modeling of slip motion at fluid-solid interfaces with heterogeneous catalysis. *Phys. Rev. Lett.* **89** (6).

Taheri, Peyman & Struchtrup, Henning 2010 An extended macroscopic transport model for rarefied gas flows in long capillaries with circular cross section. *Phys. Fluids* **22** (11), 112004.

Taheri, Peyman, Torrilhon, Manuel & Struchtrup, Henning 2009 Couette and poiseuille microflows: Analytical solutions for regularized 13-moment equations. *Phys. Fluids* **21** (1), 017102.

Tang, G. H., Gu, X. J., Barber, R. W., Emerson, D. R. & Zhang, Y. H. 2008*a* Lattice Boltzmann model for thermal transpiration. *Phys. Rev. E* **78** (2), 27701.

Tang, Guihua, Zhang, Yonghao & Emerson, David R. 2008*b* Lattice Boltzmann models for nonequilibrium gas flows. *Phys. Rev. E* **77** (4), 46701.

Tian, Zhi-Wei, Zou, Chun, Liu, Hong-Juan, Guo, Zhao-Li, Liu, Zhao-Hui & Zheng, Chu-Guang 2007 Lattice Boltzmann scheme for simulating thermal micro-flow. *Physica A* **385** (1), 59–68.

Torrilhon, Manuel & Struchtrup, Henning 2008 Boundary conditions for regularized 13-moment-equations for micro-channel-flows. *J. Comput. Phys.* **227** (3), 1982–2011.

Toro, E. F. 2009 *Riemann solvers and numerical methods for fluid dynamics*. Springer.

Toschi, F. & Succi, S. 2005 Lattice Boltzmann method at finite Knudsen numbers. *Europhys. Lett.* **69** (4), 549–555.

Wagner, Alexander J. 2008 A practical introduction to the lattice Boltzmann method.

Watari, Minoru 2009 Velocity slip and temperature jump simulations by the three-dimensional thermal finite-difference lattice Boltzmann method. *Phys. Rev. E* **79** (6), 66706.

Watari, Minoru & Tsutahara, Michihisa 2003 Two-dimensional thermal model of the finite-difference lattice Boltzmann method with high spatial isotropy. *Phys. Rev. E* **67** (3), 36306.

Yudistiawan, Wahyu P., Ansumali, Santosh & Karlin, Iliya V. 2008 Hydrodynamics beyond Navier-Stokes: The slip flow model. *Phys. Rev. E* **78** (1), 16705.

Zhang, Yonghao, Gu, Xiaojun, Barber, Robert W. & Emerson, David R. 2006 Capturing Knudsen layer phenomena using a lattice Boltzmann model. *Phys. Rev. E* **74** (4), 46704.

Zhang, Yonghao, Qin, Rongshan & Emerson, David R. 2005 Lattice Boltzmann simulation of rarefied gas flows in microchannels. *Phys. Rev. E* **71** (4), 47702.

Zheng, Lin, Guo, Zhaoli, Shi, Baochang & Zheng, Chuguang 2010 Kinetic theory based lattice Boltzmann equation with viscous dissipation and pressure work for axisymmetric thermal flows. *J. Comput. Phys.* **229** (16), 5843–5856.